

A Ku-band Multi-beam Reflectarray with 15 Beams Based on the Phase Center Reconfigurable Feed Antenna

Wenting Li, *Member, IEEE*, Chulou Yang, Yangpeng Liu, Yejun He, *Senior Member, IEEE*, Long Zhang, *Member, IEEE*, Sai-Wai Wong, *Senior Member, IEEE*, Steven Gao, *Fellow, IEEE*

Abstract—In this letter, a multi-beam reflectarray antenna operating at 16 GHz is proposed. The feed antenna contains 10 PIN diodes and 5 ports. By changing the states of the PIN diodes and exciting the corresponding port, 15 beams can be obtained. To reduce the sidelobe levels (SLLs) of the beams and achieve the broader beam coverage range (BCR), the multi-objective particle swarm optimization (MOPSO) method is introduced to optimize the reflection phase of the reflectarray. Then, the proposed reflectarray is simulated, fabricated and measured. The simulated SLL is below -9.95 dB, and the beam range is from -38.6° to 37.3°. The measured SLL is below -8.74 dB, and the beam range is from -31.5° to 30.6°.

Index Terms—Multi-beam reflectarray, reconfigurable antenna, optimization algorithm.

I. INTRODUCTION

Multi-beam reflectarrays have become popular in recent years for generating high-gain beams in different directions [1], with prospects in 5G and satellite communication [2, 3]. The phased array [4] is also capable of getting multiple beams with a high gain. However, it is costly due to the complex feeding network.

To achieve multiple beams in a reflectarray, one method is fixing the position of the feed antenna and loading components, such as PIN diodes [5] and varactor diodes [6], on elements of the reflectarray to control the reflection phase. It needs a complicated external control circuit. Another simpler method is moving the feed antenna mechanically [7] or displacing multiple feed antennas [8]. In this method, it is necessary to find a reasonable reflection phase to meet the requirement of all beams.

There are many ways to obtain the desired reflection phase. The single-focal method is used in [9, 10]. As the scanning angle increases, the SLL of the beam is higher, and the beam is wider [9]. In [11], three folded reflectarray antennas are

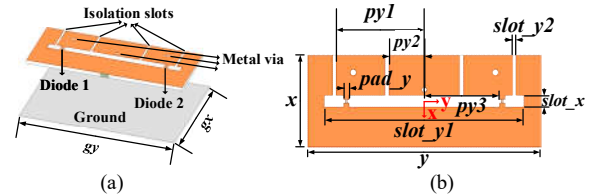
proposed using the bifocal method for improving the scanning angle. In [12], an illumination weighting factor is applied in optimizing the reflection phase for a larger beam-steering angle. The alternating projection method is implemented in [13] to generate four symmetric beams simultaneously. Global optimization algorithms, such as particle swarm optimization (PSO) and genetic algorithm (GA), are more effective in handling more complex problems [14]. In [15], the GA method is used to optimize the phase of a three-beam reflectarray. The conventional parabolic method, the bifocal method, the PSO and the multi-objective PSO (MOPSO) are discussed in [16] for beam scanning performance.

In this letter, the proposed multi-beam reflectarray contains a phase center reconfigurable feed antenna and a fixed reflecting surface. The feed antenna includes 5 slot antennas. Each is loaded by 2 PIN diodes. For a certain slot antenna, by changing the states of PIN diodes, the phase center can be moved. Thus, 3 beams of the reflectarray can be achieved by 1 port. Therefore, by exciting a certain port and changing the states of the corresponding PIN diodes, 15 beams can be realized with only 5 ports and 10 PIN diodes in the proposed reflectarray. Then, the MOPSO method is introduced to reduce the SLL and achieve a broader BCR, compared with the geometrical optics method.

II. DESIGN OF THE REFLECTARRAY

A. Phase center reconfigurable antenna

Antenna I mainly consists of a slot antenna with two PIN diodes (MADP-000907-14020x) and a ground, as shown in Fig. 1. The ground is for reducing the back lobe. The slot antenna is printed on Rogers 4003C with a thickness of 0.508 mm. The size of the slot antenna is $x \times y$, and that of the ground is $g_x \times g_y$. The distance between them is h . Four isolation slots with a width of $slot_y2$ are used to isolate DC and RF signals. Two metal vias with a radius of $r3$ are used to connect the DC bias lines. The angle of the fan-shaped area of the feed line is α , where the value of α is 120°. The fan-shaped structure of the feed line and the metal via with a radius of $r1$ are used for impedance matching. The specific parameter values of Antenna I are listed in Table I.



This work was supported in part by the National Key Research and Development Program of China under Grant 2023YFE0107900, in part by the National Natural Science Foundation of China under Grant 62101341 and Grant 62071306, and in part by the Key Program of Shenzhen Natural Science Foundation under Grant JCJY20241202124219023.

Wenting Li, Chulou Yang, Yangpeng Liu, Yejun He, Long Zhang and Sai-Wai Wong are with the State Key Laboratory of Radio Frequency Heterogeneous Integration, School of Electronic and Information Engineering, Shenzhen University, Shenzhen 518000, China.

Steven Gao is with the Department of Electronic Engineering, Chinese University of Hong Kong, Hong Kong, China.

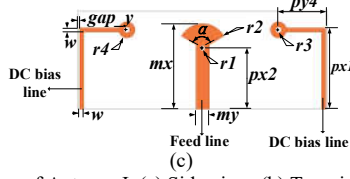


Fig. 1. The geometry of Antenna I. (a) Side view. (b) Top view. (c) Bottom view.

The current distribution of the antenna is greatly affected by the diodes. In State A, both Diode 1 and 2 are ON. In State B, Diode 1 is ON, and Diode 2 is OFF. In State C, Diode 1 is OFF, and Diode 2 is ON. The current distribution of Antenna I in the three states at 16 GHz is shown in Fig. 2, indicating a potential shift of the antenna's phase center.

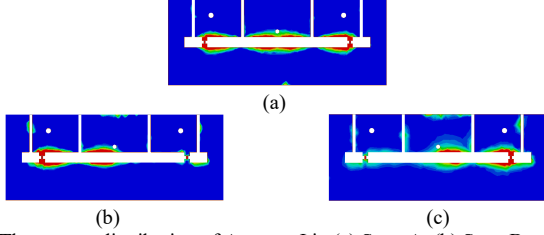


Fig. 2. The current distribution of Antenna I in (a) State A, (b) State B, and (c) State C.

TABLE I
THE PARAMETERS OF ANTENNA III (UNIT: mm)

Parameter	g_x	g_y	h	x	y	w
Value	14	20.4	6	8	20.4	0.3
Parameter	$py1$	$py2$	$py3$	$py4$	$slot_x$	pad_y
Value	7.7	3.1	6.55	4	1	0.5
Parameter	$slot_y1$	$slot_y2$	gap_y	mx	my	$px1$
Value	17.4	0.3	0.15	7	1.06	6.65
Parameter	$px2$	$r1$	$r2$	$r3$	$r4$	
Value	5	0.2	2	0.25	0.65	

To achieve a broader range of the phase center shifting, Antenna I is expanded to a multi-port feed antenna. It is shown in Fig. 3, which consists of five elements. The spacing between each element is y . The width of the antenna is increased by ex to assemble the RF connectors and the DC bias network, where ex is 12 mm. The phase center is listed in Table II when the feed antenna is in different states.

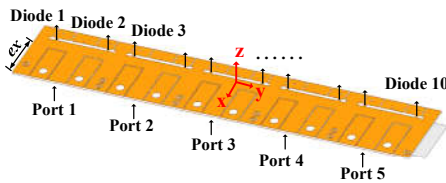


Fig. 3. The structure of the feed antenna.

TABLE II
COORDINATE OF PHASE CENTER (UNIT: mm)

State	Port (Excited)	Diode (ON)	Phase center (x, y, z)
S1	Port 5	Diode 10	(-3.12, 44.21, -0.35)
S2	Port 5	Diodes 9,10	(-2.93, 40.65, -1.27)
S3	Port 5	Diode 9	(-2.54, 36.72, -0.41)
S4	Port 4	Diode 8	(-3.21, 23.90, -0.69)
S5	Port 4	Diodes 7, 8	(-2.99, 20.33, -1.14)
S6	Port 4	Diode 7	(-2.85, 16.82, -1.02)
S7	Port 3	Diode 6	(-3.13, 3.64, -0.81)
S8	Port 3	Diodes 5,6	(-2.99, -0.04, -1.26)
S9	Port 3	Diode 5	(-3.02, -3.51, -1.18)
S10	Port 2	Diode 4	(-3.02, -16.73, -0.68)
S11	Port 2	Diodes 3,4	(-3.02, -20.37, -1.15)
S12	Port 2	Diode 3	(-3.14, -23.84, -1.16)
S13	Port 1	Diode 2	(-2.78, -36.90, -0.41)

S14	Port 1	Diodes 1, 2	(-2.93, -40.21, -2.34)
S15	Port 1	Diode 1	(-2.96, -44.57, -3.28)

B. Unit cell

The unit cell contains 5 layers, which are two layers of Rogers RO4003C, two layers of ROHACELL 31HF, and one layer of FR4. The thicknesses of them are 0.508 mm, 2 mm, and 1 mm, respectively. The unit cell is shown in Fig. 4, with a size of $a \times a$. Two patches are printed on the top and bottom surfaces of layer 1 with sizes of $l1 \times w1$ and $l2 \times w2$, respectively. The patches on the top and bottom surfaces of layer 3 are identical. Both are cut with a cross slot. The specific parameters are in Table III.

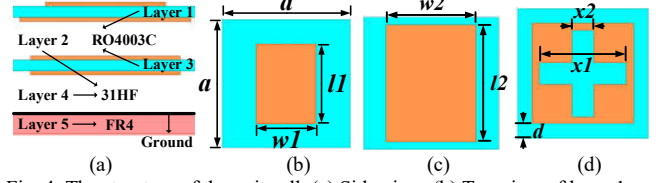


Fig. 4. The structure of the unit cell. (a) Side view. (b) Top view of layer 1. (c) Bottom view of layer 1. (d) Top/ bottom view of layer 3.

TABLE III
PARAMETERS OF UNIT CELL (UNIT: mm)

Parameter	a	$l1$	$w1$	$w2$
Value	9	$0.7 \times l2$	$0.7 \times w2$	6
Parameter	d	$x1$	$x2$	
Value	0.1	6	1.5	

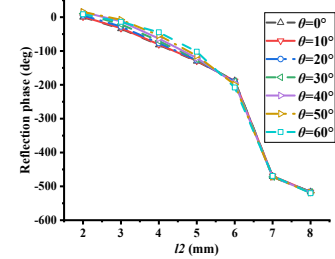


Fig. 5. Reflection phase curves under different incident angles.

When $l2$ changes, the reflection phase of the unit cell varies. The reflection phase of the unit cell under different incident angles is shown in Fig. 5. It can be observed that the difference is not significant. So, in the optimization, the phase distribution on the reflecting surface is first optimized, and then the size of the unit cell is mapped from the reflection phase curve with the incident angle being 0° .

C. Multi-Beam reflectarray antenna

By altering the state of the diode on the feed antenna and exciting a certain port, the state of the feed antenna varies, leading to the position of the phase center changing. When the reflecting surface is illuminated by the feed antenna in different states, the multi-beam reflectarray is realized. The reflecting surface is composed of 19×19 unit cells. The distance from the feed antenna to the reflecting surface is 60 mm.

III. OPTIMIZATION OF THE REFLECTION PHASE

To achieve the desired SLL, beam direction, and the expected BCR, the reflection phase of the element on the reflecting surface should be properly configured.

The geometrical optics method is a simple way [17] to calculate the required reflection phase Φ_e , which is given by

$$\Phi_e = k \cdot (\mathbf{D} - (\mathbf{X} \cdot \cos \varphi_b + \mathbf{Y} \cdot \sin \varphi_b) \cdot \sin \theta_b) \quad (1)$$

where k is the wave number in free space. (θ_b, φ_b) is the

desired beam direction. \mathbf{X} and \mathbf{Y} are the x and y coordinates of the element, and \mathbf{D} is the distance between the element and the phase center of the feed antenna. The radiation pattern \mathbf{P}^i of the reflectarray when the feed antenna is in state i can be calculated [14] by

$$\mathbf{P}^i(u, v) = \left| f_{fftshift} \left(f_{2D FFT} \left(\mathbf{A}_f^i \cdot e^{-j \cdot \Phi_f^i + j \cdot \Phi_e} \right) \right) \right| \quad (2)$$

where \mathbf{A}_f^i and Φ_f^i are the amplitude and the phase of the element's electric field receiving from the feed antenna. $f_{2D FFT}$ function is for two-dimensional Fast Fourier Transform (2D FFT), and $f_{fftshift}$ function is used to shift the zero-frequency component to the center of the spectrum.

If $\varphi_b = \frac{\pi}{2}$, $\theta_b = 0$, and the feed antenna is selected in S8, the calculated radiation pattern is shown in Fig. 6, whose BCR is from -37.1° to 37.68° . The BCR is defined as the union of the individual 3 dB beamwidths of each beam. There are two gaps in the BCR, which are from -6.35° to -5.91° and from 6.33° to 6.69° . The maximum SLL of all beams is -8.06 dB.

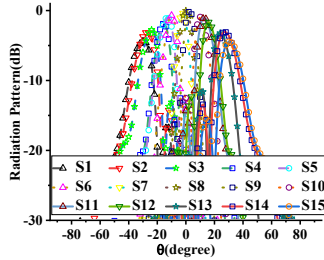


Fig. 6. The calculated radiation pattern from the geometrical optics method.

To reduce the SLL of the beam, remove the BCR gap, and extend the BCR, MOPSO is introduced to optimize the reflection phase. The fitness function $f_{fitness}$ is composed of two terms, which is given by

$$f_{fitness} = a_1 f_{2D} + a_2 f_{3D} \quad (3)$$

where a_1 and a_2 are the normalized weight coefficients. f_{2D} is a fitness function of the 2D radiation pattern, and f_{3D} is that of the 3D radiation pattern. f_{2D} is defined as

$$f_{2D} = b_1 \left(\sum_{i=1}^{15} c_1^i f_{SLL}^i + c_2^i f_{BD}^i + c_3^i f_P^i \right) + b_2 (d_1 f_{coverage} + d_2 f_{gap}). \quad (4)$$

where b_1 , b_2 , c_1^i , c_2^i , c_3^i , d_1 and d_2 are all the weight coefficients. f_{SLL}^i is a fitness function of the SLL of the beam when the feed antenna is in state i , defined as

$$f_{SLL}^i = \begin{cases} (SLL_{cal}^i - SLL_{tar}^i)^2, & SLL_{cal}^i > SLL_{tar}^i \\ 0, & SLL_{cal}^i \leq SLL_{tar}^i \end{cases} \quad (5)$$

where SLL_{cal}^i is the calculated SLL, and SLL_{tar}^i is the target SLL. f_{BD}^i is a fitness function considering the direction of the beam excited by the feed antenna in state i , which is defined as

$$f_{BD}^i = \begin{cases} (BD_{cal}^i - BD_{up}^i)^2, & BD_{cal}^i > BD_{up}^i \\ (BD_{cal}^i - BD_{low}^i)^2, & BD_{cal}^i < BD_{low}^i \\ 0, & BD_{low}^i \leq BD_{cal}^i \leq BD_{up}^i \end{cases} \quad (6)$$

where BD_{cal}^i is the calculated beam direction, and BD_{up}^i and BD_{low}^i are the upper and lower bounds of the required beam direction. f_P^i is a fitness function of the nulls of the mainlobe when the feed antenna is in state i , with the aim of obtaining a pencil-shaped beam. It is defined as

$$f_P^i = \begin{cases} (D_{cal}^i - D_{tar}^i)^2, & D_{cal}^i > D_{tar}^i \\ 0, & D_{cal}^i \leq D_{tar}^i \end{cases} \quad (7)$$

where D_{cal}^i is the calculated distance between the nulls of the mainlobe, and D_{tar}^i is the target distance of that. $f_{coverage}$ is a fitness function considering the BCR for overall beams, defined as

$$f_{coverage} = \begin{cases} (Cov_{cal} - Cov_{tar})^2, & Cov_{cal} < Cov_{tar} \\ 0, & Cov_{cal} \geq Cov_{tar} \end{cases} \quad (8)$$

where Cov_{cal} is the calculated BCR, and Cov_{tar} is the target BCR. The fitness function f_{gap} is about the gap between the adjacent beams, defined as

$$f_{gap} = \sum_{i=1}^{14} \sum_{U_{3dB}^i < L_{3dB}^{i+1}} (U_{3dB}^i - L_{3dB}^{i+1})^2 \quad (9)$$

where U_{3dB}^i is the upper bound of the beam's BCR with the feed antenna in state i , and L_{3dB}^{i+1} is the lower bound of that with the feed antenna in state $(i+1)$. f_{3D} is set to maintain the shape of the beam, defined as

$$f_{3D} = \sum_{i=1}^{15} \sum_{m=0}^M \sum_{n=0}^N \left(\mathbf{P}^i(u_m, v_n) - \mathbf{Mask}^i(u_m, v_n) \right)^2 \quad (10)$$

$\mathbf{P}^i(u_m, v_n) > \mathbf{Mask}^i(u_m, v_n),$
 $(u_m, v_n) \in \text{visible range}$

where (u_m, v_n) is a discrete point in the u-v domain. M and N are both the number of points used for the 2D FFT. \mathbf{Mask}^i is the mask in the visible range with the feed antenna in state i , which is defined as

$$\mathbf{Mask}^i = \begin{cases} 0, & (u - u_0^i)^2 + (v - v_0^i)^2 \leq r_0^2 \\ M_i, & (u - u_0^i)^2 + (v - v_0^i)^2 > r_0^2 \end{cases} \quad (11)$$

where (u_0^i, v_0^i) is the desired beam direction in the u-v domain. For example, \mathbf{Mask}^5 is shown in Fig. 7.

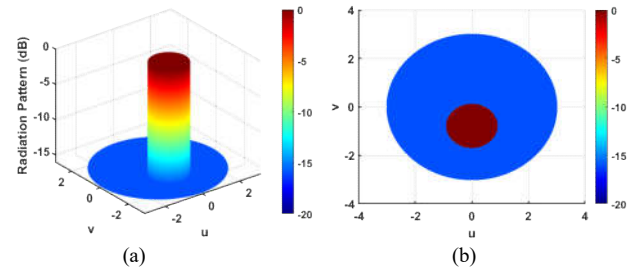


Fig. 7. \mathbf{Mask}^5 in the visible range. (a) Side view. (b) Top view.

In (1), \mathbf{X} and \mathbf{Y} are fixed. When the feed antenna is in state i , \mathbf{D}^i is the distance between the element and the phase center of the feed antenna, and the required reflection phase Φ^i is determined by the beam direction (θ^i, φ^i) , written as

$$\Phi^i(\theta^i, \varphi^i) = k \cdot (\mathbf{D}^i - (\mathbf{X} \cdot \cos \varphi^i + \mathbf{Y} \cdot \sin \varphi^i) \cdot \sin \theta^i) \quad (12)$$

Although there are 15 states in the antenna, only one reflection phase distribution exists on the reflecting surface. For the q^{th} particle in p^{th} iteration, the reflection phase $\Phi(q)^{(p)}$ is given by

$$\Phi(q)^{(p)} = (\Phi_{\Delta}(q)^{(p)} + \sum_{i=1}^{15} w_i(q)^{(p)} \cdot \Phi^i(\theta_i(q)^{(p)}, \varphi_i(q)^{(p)})) \quad (13)$$

where w_i is the normalized weight coefficient, and Φ_{Δ} is a matrix whose elements can vary from 0 to π . Here, Φ_{Δ} , w_i , θ_i , and φ_i are the variables needed to be optimized. To reduce the

number of the variables, only a quarter of the elements of the reflectarray are taken into account, with the reflection phase distribution being symmetric.

The optimized radiation patterns are shown in Fig. 8. The BCR is from -41.32° to 40.94° with no gap, and the maximum SLL of all beams is -10.27 dB.

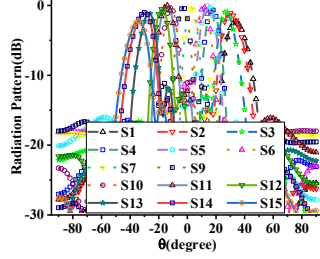


Fig. 8. The optimized radiation pattern.

IV. SIMULATED AND MEASURED RESULTS

The optimized reflectarray antenna is simulated, fabricated, and measured. The prototype is shown in Fig. 9.

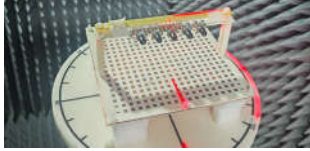


Fig. 9. The prototype of the proposed antenna.

The reflection coefficient of the proposed reflectarray is displayed in Fig. 10. The simulated reflection coefficient is below -10 dB from 15.36 to 17 GHz, and the measured one is below -10 dB from 15.16 to 16.77 GHz.

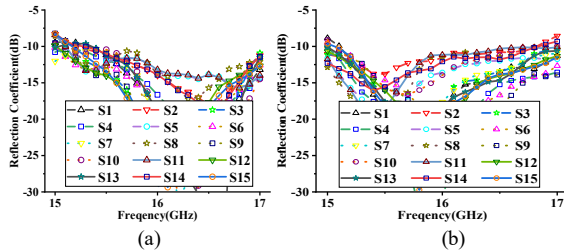


Fig. 10. (a) The simulated reflection coefficient and (b) the measured reflection coefficient.

The simulated and measured radiation patterns at 16 GHz are displayed in Fig. 11. The simulated maximum SLL is -9.95 dB, and the beam range is from -38.6° to 37.3° . The measured maximum SLL is -8.74 dB, and the beam range is from -31.5° to 30.6° .

The gain of the proposed reflectarray is displayed in Fig. 12. For most states, the peak gain appears at 16.1 GHz. The measured maximum aperture efficiency is 11.75% at 16.4 GHz.

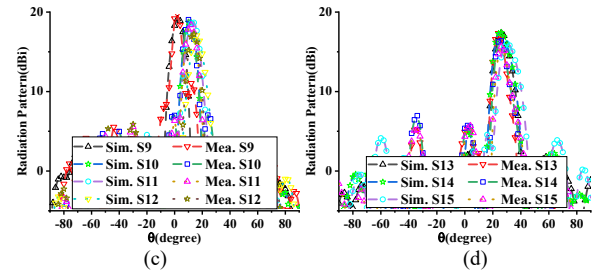
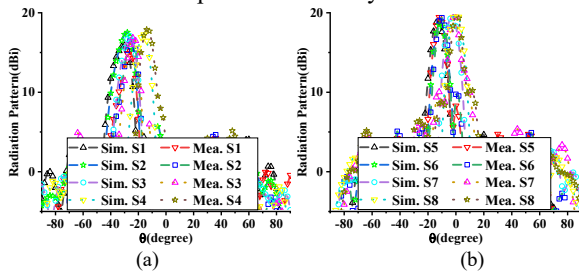


Fig. 11. The simulated and the measured radiation patterns at 16 GHz.

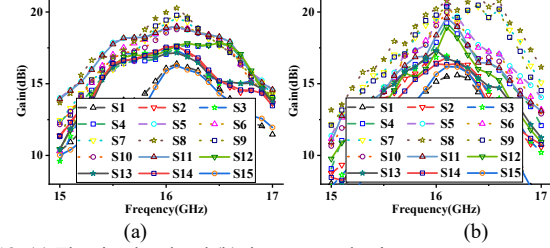


Fig. 12. (a) The simulated and (b) the measured gain.

The proposed multi-beam reflectarray is compared with the existing works, which is shown in Table IV. To achieve a certain number of electronic switching beams, the proposed reflectarray employs the least ports.

TABLE IV

THE PERFORMANCE COMPARISON BETWEEN DIFFERENT WORKS

	Number of ports	Number of beams	Beam switching method	Scan range	Maximum aperture efficiency
Ref. [7]	1	5	Mechanical moving	-14.6° to 14.9°	19.45%
Ref. [11]	21	19	Electronic switching	-30° to 30°	3.48%
Ref. [12]	15	15	Electronic switching	-29° to 29°	15%
Ref. [18]	1	7	Mechanical moving	-45° to 45°	36%
This work	5	15	Electronic switching	-38.6° to 37.3°	13.72%

V. CONCLUSION

In this letter, a multi-beam reflectarray is proposed. The phase center of the feed antenna can be changed by altering the states of the PIN diodes. 15 beams can be obtained in total. Then, to attain lower SLL and a broader beam range, MOPSO is introduced. The simulated impedance bandwidth is from 15.36 to 17 GHz, and the measured one is from 15.16 to 16.77 GHz. The simulated and measured isolation is below -20 dB from 15 to 17 GHz. The SLLs of the beams are below -9.95 dB in the simulated radiation patterns, and those are below -8.74 dB in the measured ones. The simulated beam range is from -38.6° to 37.3° , while the measured one is from -31.5° to 30.6° . When switching the beams, the simulated gain varies from 15.89 to 19.96 dBi at 16 GHz, and the measured one changes from 15.15 to 20.21 dBi.

REFERENCES

- [1] P. Nayeri, F. Yang, and A. Z. Elsherbeni, "Beam-Scanning Reflectarray Antennas: A technical overview and state of the art," *IEEE Antennas Propag. Mag.*, vol. 57, pp. 32-47, 2015.
- [2] J. M. Wen, C. K. Wang, W. Hong, Y. M. Pan, and S. Y. Zheng, "A Wideband Switched-Beam Antenna Array Fed by Compact Single-

- Layer Butler Matrix," *IEEE Trans. Antennas Propag.*, vol. 69, pp. 5130-5135, 2021.
- [3] Y.-E. Chi, J. Park, and S.-O. Park, "Hybrid Multibeamforming Receiver With High-Precision Beam Steering for Low Earth Orbit Satellite Communication," *IEEE Trans. Antennas Propag.*, vol. 71, pp. 5695-5707, 2023.
- [4] M. Liu, F. Lin, and H. J. Sun, "Broadband Frequency-Independent Beamforming Networks for Multibeam Antenna Arrays," *IEEE Antennas Wireless Propag. Lett.*, vol. 22, pp. 2397-2401, 2023.
- [5] E. Carrasco, M. Barba, and J. A. Encinar, "X-Band Reflectarray Antenna With Switching-Beam Using PIN Diodes and Gathered Elements," *IEEE Trans. Antennas Propag.*, vol. 60, pp. 5700-5708, 2012.
- [6] L. Boccia, G. Amendola, and G. Di Massa, "Performance Improvement for a Varactor-Loaded Reflectarray Element," *IEEE Trans. Antennas Propag.*, vol. 58, pp. 585-589, 2010.
- [7] I. Y. Tarn, Y.-S. Wang, and S.-J. Chung, "A Dual-Mode Millimeter-Wave Folded Microstrip Reflectarray Antenna," *IEEE Trans. Antennas Propag.*, vol. 56, pp. 1510-1517, 2008.
- [8] W. Menzel, M. Al-Tikriti, and R. Leberer, "A 76 GHz multiple-beam planar reflector antenna," *the 32nd Eur. Microw. Conf.*, Milano, Italy, Sep. 2002.
- [9] S. R. Rengarajan, "Scanning and Defocusing Characteristics of Microstrip Reflectarrays," *IEEE Antennas Wireless Propag. Lett.*, vol. 9, pp. 163-166, 2010.
- [10] M. Jiang, W. Hong, Y. Zhang, S. Yu, and H. Zhou, "A Folded Reflectarray Antenna With a Planar SIW Slot Array Antenna as the Primary Source," *IEEE Trans. Antennas Propag.*, vol. 62, pp. 3575-3583, 2014.
- [11] Y. Hu, W. Hong, and Z. H. Jiang, "A Multibeam Folded Reflectarray Antenna With Wide Coverage and Integrated Primary Sources for Millimeter-Wave Massive MIMO Applications," *IEEE Trans. Antennas Propag.*, vol. 66, pp. 6875-6882, 2018.
- [12] Z.-Y. Yu, Y.-H. Zhang, S.-Y. He, H.-T. Gao, H.-T. Chen, and G.-Q. Zhu, "A Wide-Angle Coverage and Low Scan Loss Beam Steering Circularly Polarized Folded Reflectarray Antenna for Millimeter-Wave Applications," *IEEE Trans. Antennas Propag.*, vol. 70, pp. 2656-2667, 2022.
- [13] P. Nayeri, F. Yang, and A. Z. Elsherbeni, "Design and Experiment of a Single-Feed Quad-Beam Reflectarray Antenna," *IEEE Trans. Antennas Propag.*, vol. 60, pp. 1166-1171, 2012.
- [14] P. Nayeri, F. Yang, and A. Z. Elsherbeni, "Design of Single-Feed Reflectarray Antennas With Asymmetric Multiple Beams Using the Particle Swarm Optimization Method," *IEEE Trans. Antennas Propag.*, vol. 61, pp. 4598-4605, 2013.
- [15] C. Yang, W. Li, Y. He, L. Zhang, and S.-W. Wong, "A Multi-beam Reflectarray Antenna with the Genetic Algorithm Optimizing Beams," presented at the 2023 16th UK-Europe-China Workshop on Millimetre Waves and Terahertz Technologies, 2023.
- [16] P. Nayeri, F. Yang, and A. Z. Elsherbeni, "Bifocal Design and Aperture Phase Optimizations of Reflectarray Antennas for Wide-Angle Beam Scanning Performance," *IEEE Trans. Antennas Propag.*, vol. 61, pp. 4588-4597, 2013.
- [17] J. Huang and J. A. Encinar, *Reflectarray Antennas (John Wiley & Sons)*. 2008.
- [18] G. B. Wu, S. W. Qu, and S. Yang, "Wide-Angle Beam-Scanning Reflectarray With Mechanical Steering," *IEEE Trans. Antennas Propag.*, vol. 66, pp. 172-181, 2018.